Heliyon 10 (2024) e39076

Contents lists available at ScienceDirect

Heliyon

journal homepage: www.cell.com/heliyon

Research article

Remote ischemic preconditioning plays a neuroprotective role in cerebral ischemia-reperfusion mice by inhibiting mitophagy

Jiayi Zhu [a,1], Na Xu [a,1], Heng Lin [a,1], Li Deng [a], Bingqing Xie [b], Xiaoqian Jiang [a], Runde Liao [a], Chaoxian Yang [a,*]

[a] Department of Anatomy, School of Basic Medical Sciences, Southwest Medical University, Luzhou, China
[b] Laboratory of Neurological Diseases and Brain Function, the Affiliated Hospital of Southwest Medical University, Luzhou, China

ARTICLE INFO

Keywords:
Remote ischemic preconditioning
Cerebral ischemia-reperfusion
Mitophagy

ABSTRACT

Remote ischemic preconditioning (RIPC) represents a clinically feasible method for safeguarding vital organs against ischemic injury. However, its specific role in cerebral ischemia-reperfusion (I/R) injury remains to be definitively elucidated. In this study, we investigated the neuroprotective effects of RIPC on mice at 7 days post-cerebral I/R and its involvement in mitophagy and mitochondrial dysfunction. Cerebral I/R led to impaired brain function, as well as structural and functional damage to mitochondria. Notably, RIPC treatment ameliorated the neurological dysfunction induced by cerebral I/R. Compared with the I/R group, the expression levels of NeuN, MBP, PDH, and Tom20 were significantly elevated in the RIPC + I/R group. Furthermore, mitochondria in the RIPC + I/R group exhibited more intact structure compared to those in the I/R group. In mice subjected to I/R injury, RIPC treatment markedly increased ATP content, ADP content, TAN level and glucose uptake while upregulating expression levels of Parkin, Pink1 and P62 proteins; it also reduced both the volume of ischemic foci and the number of mitochondrial autophagosomes along with decreasing LC3B II/I ratio. In conclusion, RIPC may exert a neuroprotective role by inhibiting excessive mitophagy during subacute stages following an ischemic stroke.

1. Introduction

Currently, the management of ischemic stroke encompasses pharmacological, surgical, interventional, and acupuncture interventions [1–3]. However, these approaches represent artificial rescue measures post-stroke and may not yield immediate efficacy. Activation of the organism's endogenous active resistance has the potential to mitigate disease severity prior to human intervention. Induced ischemia tolerance is a strategy aimed at exploring endogenous protective measures against ischemic stroke, with ischemic preconditioning being the most prevalent method [4]. Remote ischemic preconditioning (RIPC) presents easier and less risky than ischemic preconditioning targeting the heart or brain [5,6]. In clinical application, RIPC typically involves utilizing a blood pressure cuff to intermittently compress and release the patient's limbs, leading to transient limb ischemia. This process can trigger the body's endogenous protective response, thereby attenuating the damage caused by subsequent severe or fatal ischemia in vital organs [7,8].

The protective mechanism of RIPC on ischemic organs primarily involves the following aspects: stimulating autonomic nervous

* Corresponding author.
E-mail address: lyycx@foxmail.com (C. Yang).
[1] These authors contributed equally to the article: Jiayi Zhu, Na Xu, Heng Lin.

https://doi.org/10.1016/j.heliyon.2024.e39076
Received 14 March 2024; Received in revised form 25 September 2024; Accepted 7 October 2024
Available online 10 October 2024

system activity, suppressing inflammatory response, inhibiting oxidative stress response, influencing hemodynamics and coagulation response, reducing cell apoptosis, and regulating cellular energy metabolism and amino acid metabolism [9–13]. Nevertheless, the efficacy and potential neuroprotective mechanism of RIPC as an intervention in cases of ischemic stroke remain to be observed.

Cerebral ischemia-reperfusion (I/R) can result in extensive cellular damage within the ischemic area. Cellular damage affects proteins, lipids, DNA, and other components within mitochondria, leading to structural abnormalities and functional disorders. The mitochondrial quality control (MQC) facilitates restoration of normal mitochondrial structure or removal of aberrant components [14]. Mitophagy is a crucial process in MQC. It selectively removes excessive or damaged mitochondria, thereby effectively regulating the cellular mitochondrial quantity and maintaining their normal function [15]. Some studies have demonstrated that the promotion of mitophagy can mitigate ischemia-reperfusion injury (IRI) [16–18]. However, this phenomenon is a double-edged sword, as excessive mitochondrial autophagy may exacerbate mitochondrial dysfunction and promote cell apoptosis [19,20]. In mice, the loss of uncoupling protein 2 aggravates cerebral I/R injury by enhancing mitophagy and cell apoptosis [21].

In this investigation, we explored whether mitophagy is involved in the neuroprotective effects of RIPC against cerebral IRI. It is expected to provide potential information for elucidating the mechanism of RIPC in preventing ischemic stroke.

2. Results

2.1. RIPC improves neurological function

Both the I/R and RIPC + I/R groups exhibited evident symptoms of neurological impairment 2 h after I/R, including positive tail lifting test results, turning or tipping during ambulation, decreased sensation, reduced balance, and absent reflexes. The mNSS score for each mouse was greater than or equal to 9; however, there was no significant difference in mNSS score between the I/R and RIPC + I/R groups. No symptoms of neurological injury were observed at the same time point in the Sham group or the RIPC group (Fig. 1A–B). On day 9, the mNSS scores of the I/R and RIPC + I/R groups were significantly higher than those of the Sham and RIPC groups, nevertheless, the score of the RIPC + I/R group was notably lower than that of the I/R group ($P < 0.05$, Fig. 1C).

In this study, the footprints and strides of mice exhibited significant changes following I/R (Fig. 2A–B). Gait analysis demonstrated a decrease in the regularity index of normal step sequence, run speed, print area, stride lengths, and stance time, along with an increase in the swing time after I/R ($P < 0.05$, Fig. 2C–N). Conversely, RIPC treatment was associated with notable improvements in the regularity index of normal step sequence, run speed, print area, stride lengths (front left paw (FL), front right paw (FR), and rear right paw (RR)), as well as increased stance time for rear left paw (RL)/RR; meanwhile there were decreases in the swing time among I/R mice ($P < 0.05$, Fig. 2C–N).

2.2. RIPC improves the pathological structure of the brain

Brain tissues of mice from the Sham and RIPC groups exhibited red with TTC staining, while the right cerebral tissues of mice from the I/R and RIPC + I/R groups displayed distinct white ischemic areas (Fig. 3A). The volume of the infarct area was significantly reduced in the RIPC + I/R group compared to that in the I/R group ($P < 0.05$, Fig. 3B). HE staining revealed normal brain structures in

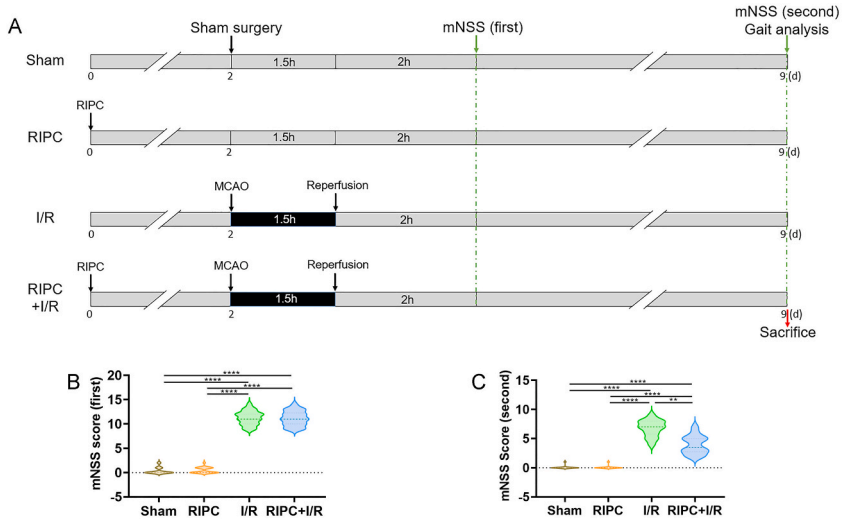

Fig. 1. Neurological function evaluated using the mNSS test. (A) Brief timelines of the experimental procedures depict the time points for the gait analysis, as well as first and second mNSS tests. (B–C) Neurological function scores at different time points are presented for each group. Data are represented as mean ± SD (B: n = 22; C: n = 14). ****$P < 0.0001$ as determined with repeated measures one-way ANOVA (Tukey's multiple comparison test).

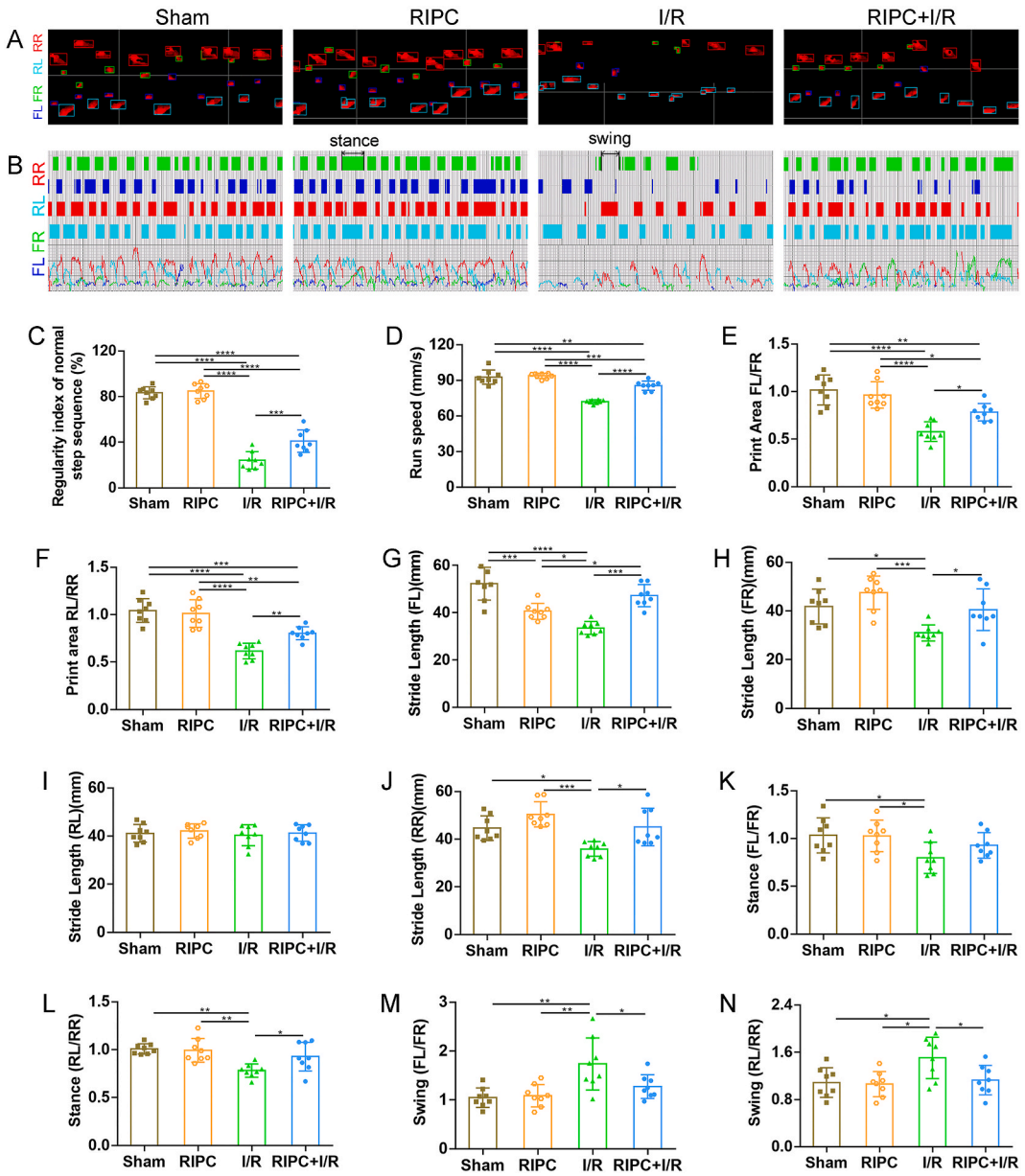

Fig. 2. Neurological function evaluated using a passive gait analysis system. (A) Representative paw prints of the mice in the different groups. (B) Representative strides of the mice in the different groups. (C–N) Gait parameters, including the regularity index of normal step sequence, running speed, print area, stride length, stance and swing time, were analyzed using GAIT SCAN analysis software. Data are presented as mean ± SD (C–N: n = 8). $^{*}P < 0.05$, $^{**}P < 0.01$, $^{***}P < 0.001$, $^{****}P < 0.0001$ as determined with ordinary one-way ANOVA (Tukey's multiple comparison test).

mice from the Sham and RIPC groups, whereas those in the I/R group showed a sparse distribution of cells and cellular swelling. Moreover, the tissue structure analysis indicated that peri-ischemic area in the RIPC + I/R group was more complete and denser than that in the I/R group (Fig. 3C). Nissl staining demonstrated that the staining area of Nissl bodies at the margin of ischemia in the I/R group were lower than those in the sham and RIPC groups ($p < 0.05$). However, RIPC treatment significantly increased Nissl staining area ($p < 0.05$, Fig. 3D–E). TUNEL staining revealed minimal apoptotic cells in the Sham and RIPC groups, while the number of apoptotic cells in the I/R and RIPC + I/R groups was significantly increased, and the apoptosis rate of the RIPC + I/R group was significantly decreased compared with that of the I/R group ($P < 0.05$, Fig. 3F–G).

2.3. RIPC reduces brain injury

Immunofluorescence staining and TEM were utilized to observe the neurons and the myelin sheath. There was no statistical

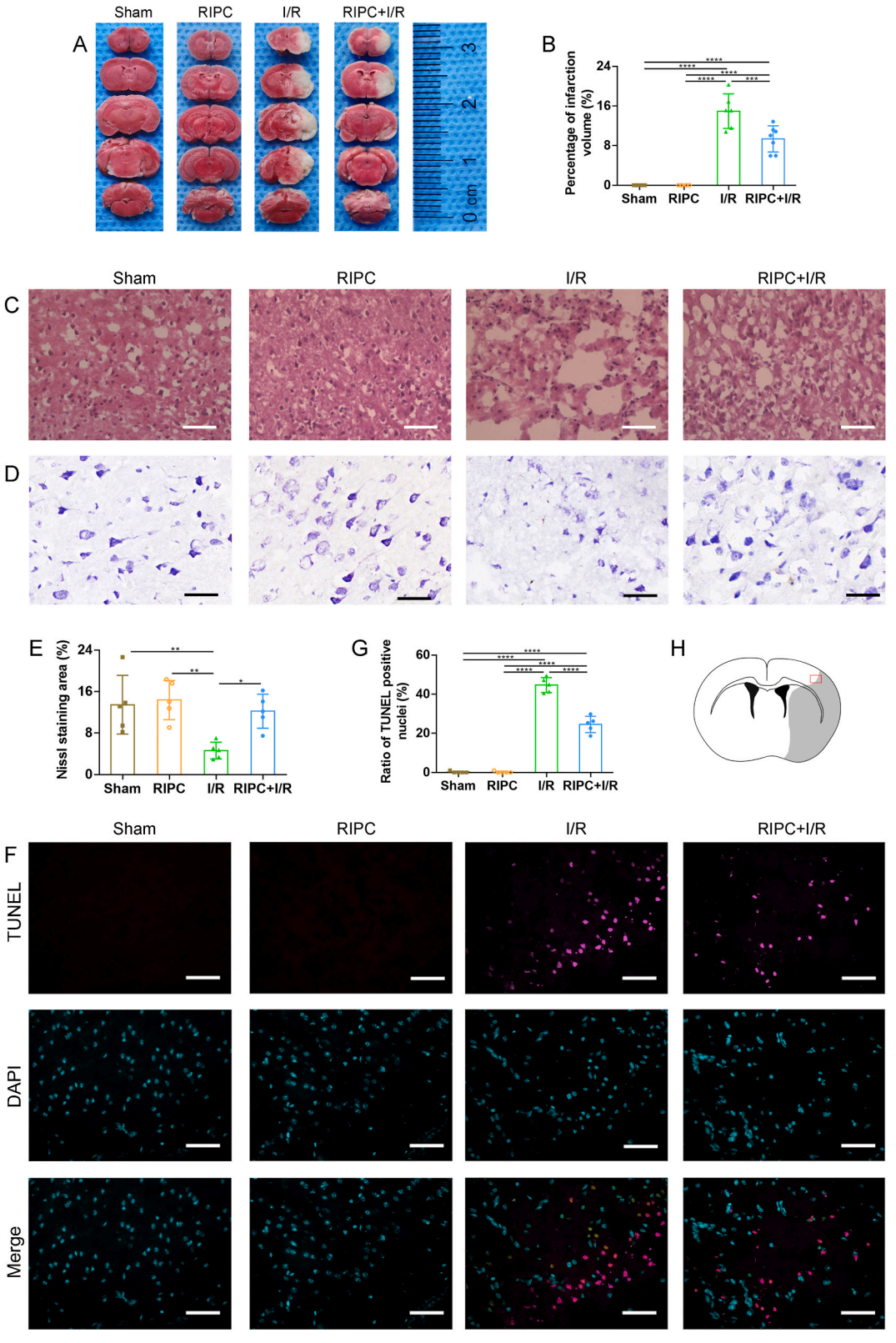

(caption on next page)

Fig. 3. Pathological characteristics of brain tissue. (A) TTC staining reveals infarct areas. (B) Quantification of infarct volumes in the different groups. (C) HE staining shows the histopathological structure of the brain tissue in the different groups. (D) Nissl staining displays the Nissl bodies in the different groups. (E) Quantification of Nissl staining area at the margin of ischemia for each group. (F) Representative images of TUNEL staining for each group. (G) Statistical results regarding apoptosis rate in each group. (H) The red box in the illustration depicts the regions of interest (ROI) in Fig. 3C–D,F. Shadow outline the infarct area. Data are presented as mean ± SD (B: n = 6–7; E, G: n = 5). Bar = 100 μm (C, F) or 50 μm (D). *$P < 0.05$, **$P < 0.01$, ****$P < 0.0001$ as determined with ordinary one-way ANOVA (Tukey's multiple comparison test).

difference in the ratio of NeuN-positive cells or fluorescence intensity of MBP between the Sham and RIPC groups. Compared with those in the Sham and RIPC groups, the ratio of NeuN-positive cells and fluorescence intensity of MBP decreased significantly in the I/R group ($P < 0.05$, Fig. 4A–D). However, there was a notable increase in both parameters in the RIPC + I/R group compared to the I/R group ($P < 0.05$, Fig. 4A–D). Additionally, TEM revealed intact neuron and myelin structures in the Sham and RIPC groups, while neuronal edema and myelin rupture or demyelination occurred after cerebral I/R; these effects were mitigated in the RIPC + I/R group (Fig. 4E–G).

2.4. RIPC increases glucose uptake

Micro-PET–CT scan was utilized to evaluate glucose metabolism and infarct volume in mouse brains subjected to I/R (Fig. 5A). These results revealed the absence of ischemic foci in the Sham and RIPC groups, while obvious ischemic foci were observed in mice after cerebral I/R. However, the ischemic volume was significantly smaller in the RIPC + I/R group compared to the I/R group ($P < 0.05$, Fig. 5B). In addition, glucose metabolism levels were notably lower in the I/R and RIPC + I/R groups than those in the Sham and RIPC groups; nevertheless, they were higher in the RIPC + I/R group than in the I/R group ($P < 0.05$, Fig. 5C).

2.5. RIPC improves the structure and function of mitochondria

The ultrastructure of mitochondria in the ischemic penumbra was examined using TEM. The images showed that the mitochondrial membrane and crests in the Sham and RIPC groups were intact, with minimal occurrence of mitochondrial vacuolation. Conversely, the I/R group exhibited mitochondrial vacuolation, crest fracture and dissolution (Fig. 6A). In comparison to the I/R group, the RIPC + I/R group demonstrated an increased number of mitochondria, a more complete structure, and clearer mitochondrial cristae ($P < 0.05$, Fig. 6C–D).

To gain deeper insights into mitochondrial function, we conducted liquid chromatography to analyze the levels of ATP, ADP, and AMP in the brain tissues. Fig. 6E illustrates the chromatograms of ATP, ADP, and AMP obtained under specific chromatographic conditions. By utilizing a concentration series of standard solutions, we generated standard curved and derived the following regression equations: ATP: $Y = 5.48 \times 10^{-8}x+1.69 \times 10^{-4}$, $R^2 = 0.998$; ADP: $Y = 6.09 \times 10^{-8}x-8.38 \times 10^{-4}$, $R^2 = 0.999$; AMP: $Y = 5.21 \times 10^{-8}x-3.49 \times 10^{-4}$, $R^2 = 0.999$. We calculated the levels of ATP, ADP, and AMP as well as their sum (total adenine nucleotide (TAN)). Compared with those in the Sham and RIPC groups, the levels of ATP, ADP, AMP, and TAN were significantly lower in the I/R group; however, the RIPC treatment markedly increased the levels of ATP, ADP, and TAN in I/R mice ($P < 0.05$, Fig. 6F–I).

2.6. RIPC mitigates mitochondrial damage

Furthermore, immunofluorescence staining and Western blotting were employed to detect the expression of the mitochondrial proteins PDH and Tom20 (Fig. 7A–B, F). The findings revealed no significant differences in the expression levels of PDH and Tom20 between the Sham and RIPC groups; however, these levels were notably reduced in the I/R group. Additionally, the expression of PDH and Tom20 in the RIPC + I/R group exhibited a significant increase compared to that in the I/R group ($P < 0.05$, Fig. 7).

2.7. RIPC inhibits mitophagy

In this study, the presence of mitochondrial autophagosomes was confirmed by dual labeling immunofluorescence of pyruvate dehydrogenase (PDH) on the mitochondria and LC3B on the autophagosome, as shown in Fig. 8A. The number of mitochondrial autophagosomes was markedly higher in the I/R group compared to those in the Sham and RIPC groups. Additionally, in compared to the I/R group, there was a moderate decrease in the number of mitochondrial autophagosomes in the RIPC + I/R group ($P < 0.05$, Fig. 8B). Fig. 8C illustrated a mitochondrial autophagosome adjacent to the mitochondria in a mouse brain following I/R. Moreover, Western blotting was used to assess the expression of autophagy-related proteins. The results showed that there were no significant differences in PINK1, Parkin, P62, and LC3 protein levels between the Sham group and RIPC groups. In contrast, lower expression levels of PINK1, Parkin, and P62 proteins were observed in the I/R group compared to both Sham and RIPC groups; however, an increase was noted in LC3 II/I ratio ($P < 0.05$, Fig. 8E–I). In comparison with those from I/R group samples, increased expression levels of Parkin, PINK1, and P62 proteins but decreased LC3 II/I ratio were observed for samples from RIPC + I/R group ($P < 0.05$, Fig. 8E–I).

3. Discussion

Ischemic preconditioning is a technique that activates the endogenous protective mechanism of "ischemia tolerance". It involves

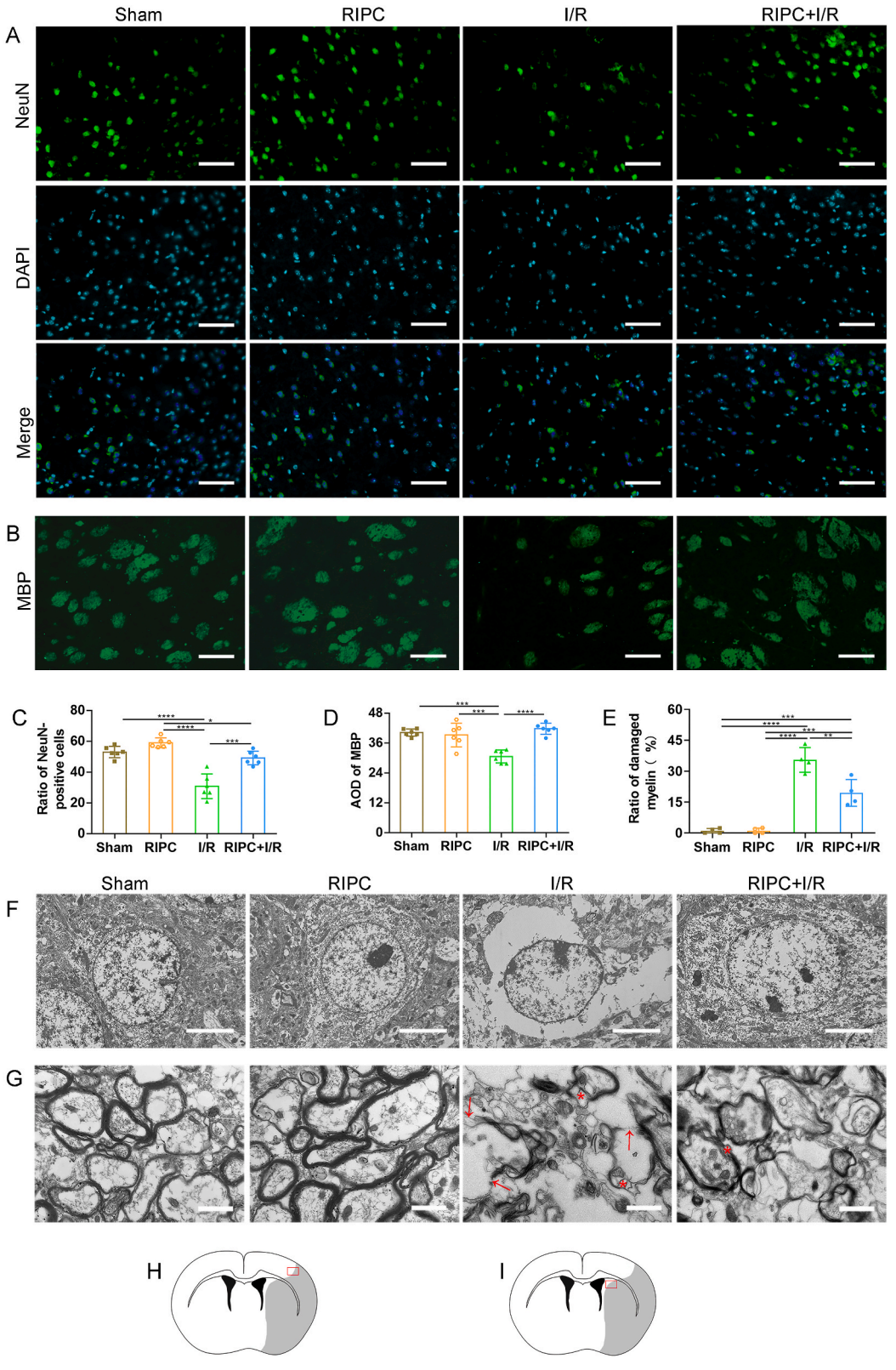

(caption on next page)

Fig. 4. RIPC improves neuron and myelin sheath. (A) Representative images of NeuN immunofluorescence staining for the different groups. (B) Representative images of MBP immunofluorescence staining for the different groups. (C–D) Statistical results of NeuN and MBP immunofluorescence staining. (E) Representative electron micrographs of neurons in the different groups. (F) Representative electron micrographs of the myelin sheath in the different groups. The red arrow points to myelin rupture, and the red star indicates demyelination. (G) Statistical results of damaged myelin. (H) The red box in the illustration depicts the ROI in Fig. 4A–E. (I) The red box in the illustration depicts the ROI in Fig. 4B–F. Data are presented as mean ± SD (C–D: n = 5; E: n = 4). Bar = 100 μm (A) or 5 μm (B) or 50 μm (C) or 1 μm (D). $^{*}P < 0.05$, $^{**}P < 0.01$, and $^{***}P < 0.001$ as determined with ordinary one-way ANOVA (Tukey's multiple comparison test).

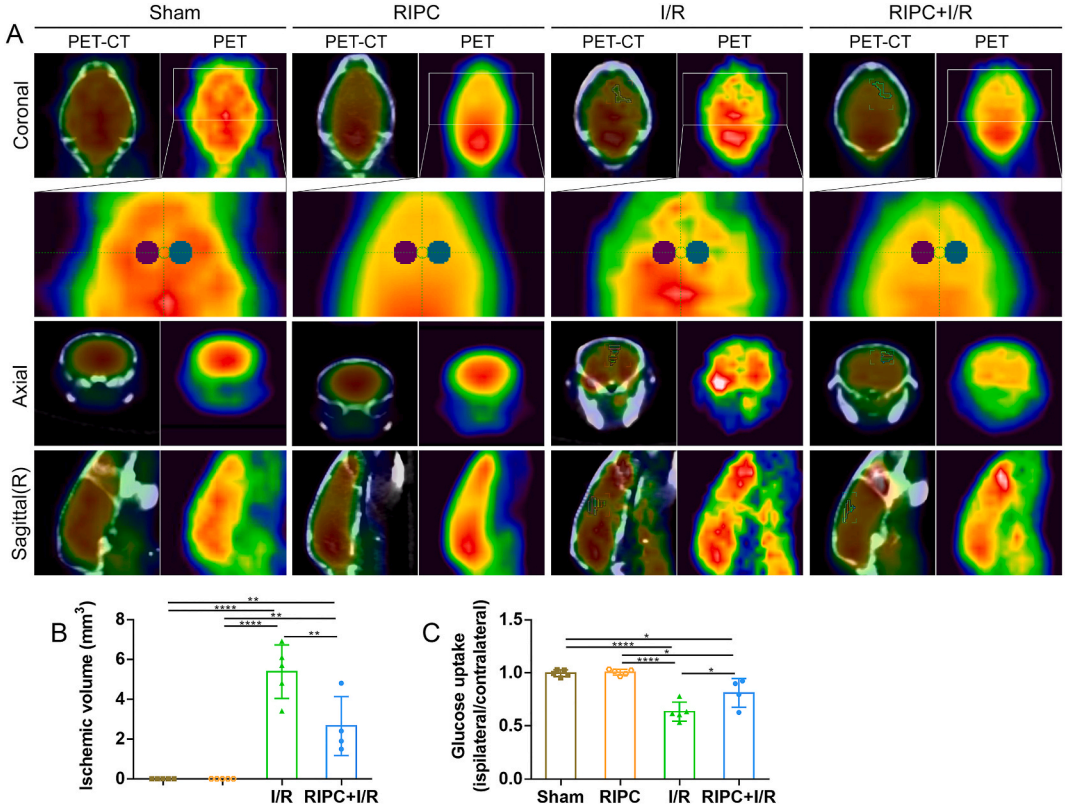

Fig. 5. RIPC reduces the volume of ischemic foci and improved the level of glucose uptake. (A) Representative PET-CT images of the mouse brains from the I/R and RIPC + I/R groups. The shadow represents the ischemic focus, while circular points represent the checkpoints of glucose uptake. (B–C) Quantitative analysis results for the volume of ischemic foci (B) and glucose uptake (C) using PET–CT scanning. Data are presented as mean ± SD (B–C: n = 4–5). $^{*}P < 0.05$ as determined with ordinary one-way ANOVA (Tukey's multiple comparison test).

two protective stages, one early and one late. The early phase may develop within minutes of the initial ischemic injury and last for 2–3 h. The late phase becomes apparent after 12–24 h and lasts for 3–4 days, providing protection against both infarction and stunning [22]. RIPC can provide neuronal mediated protection against endothelial I/R injury at 24 h and 48 h [23]. Previous experiments have confirmed that RIPC administration 48 h prior to cerebral I/R significantly protects the brain [13]. Therefore, in this study, animals in the RIPC + I/R group underwent I/R surgery two days after RIPC.

The extent of brain injury following I/R can be assessed using various methodologies [13,24]. In this study, the neurological function recovery of mice in the RIPC + I/R group was superior to that of mice in the I/R group, as evidenced by mNSS scores and gait analyses. TTC staining showed that the white infarct areas were predominantly located in the cortex, corpus callosum, striatum, and thalamus of the right brain tissue post-cerebral I/R. These white areas reflect reduced dehydrogenase activity and cell physiological dysfunction within these regions. Notably, compared to the I/R group, a smaller white infarct area was observed in the RIPC + I/R group. Furthermore, ^{18}F-FDG micro-PET/CT scans demonstrated a smaller volume of ischemic area in the RIPC + I/R group than in the I/R group. These findings indicate a close relationship between lesion area reduction and improved neurological function.

Nissl bodies play a crucial role in synthesizing structural proteins necessary for the regeneration of organelles, enzymes required for neurotransmitter synthesis, and neural modulators, which can be used as indicators of neuronal functional status [25–27]. Compared to the Sham and RIPC groups, it was observed that the Nissl staining area decreased and exhibited blurred boundaries in the I/R group. However, when compared to the I/R group, the Nissl staining area increased in the RIPC + I/R group and displayed clearer morphology. This finding suggests that neuronal protein synthesis function declines after I/R but can be enhanced by RIPC treatment

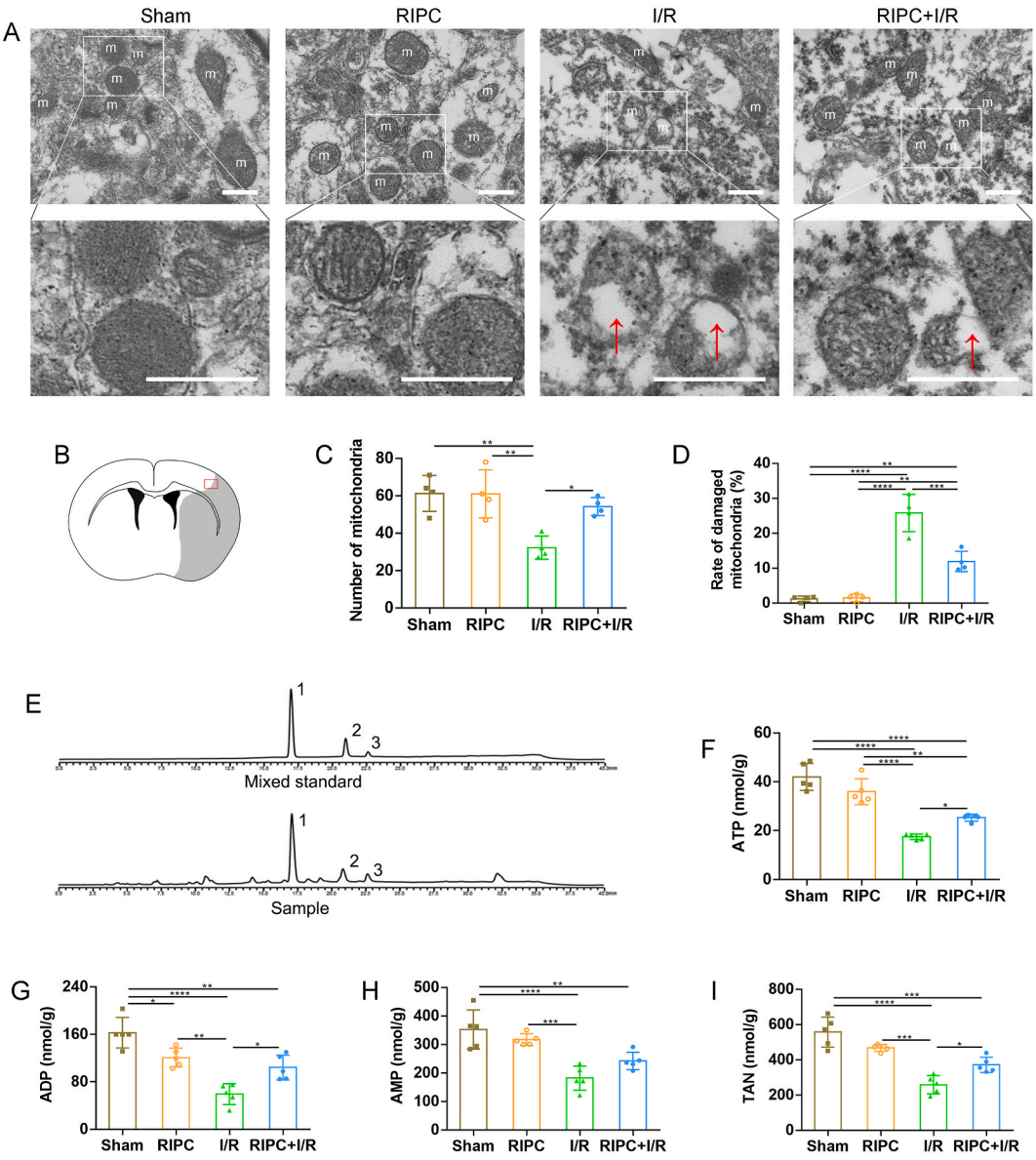

Fig. 6. RIPC improves mitochondrial quality in I/R mice. (A) Representative images of mitochondria in different groups. The red arrow points to a damaged mitochondrion. (B) The red box in the illustration depicts the ROI in Fig. 6A. (C) The number of mitochondria was quantified for each experimental groups. (D) The percentage of damaged mitochondria was calculated for each experimental groups. (E) Chromatogram of mixed standard and sample. 1: AMP; 2: ADP; 3: ATP. (F–I) Statistical results of ATP, ADP, AMP and TAN contents in brain tissue. Data are presented as mean ± SD (C–D: n = 4; F–I: n = 5). Bar = 500 nm $^{*}P < 0.05$, $^{**}P < 0.01$, $^{***}P < 0.001$, $^{****}P < 0.0001$ as determined with ordinary one-way ANOVA (Tukey's multiple comparison test).

prior to I/R, providing some support for the locomotion gait results.

NeuN (neuron marker) immunohistochemical staining and TUNEL staining have been widely employed for assessing infarct development in MCAO animal models [28–30]. In this study, the ratio of NeuN–immunopositive cells decreased while the ratio of apoptotic cells increased following I/R, but this change was partially reversed by RIPC treatment before I/R. Furthermore, previous reports have indicated stroke-induced oligodendrocyte degeneration and demyelination [31,32], whereas our findings demonstrate elevated level of MBP (oligodendrocyte maturation-associated protein) in the RIPC + I/R group compared to the I/R group. These results suggest that RIPC exerts a protective effect on neurons and white matter, serving as the cytological basis for reducing the infarct size and improving neurological impairment symptoms in I/R mice.

Research findings have demonstrated an association between diminished glucose uptake within specific regions of the brain and impaired functionality, which is common in stroke disease [33,34]. PET/CT imaging revealed a significant decrease in focal area glucose uptake following cerebral I/R, RIPC intervention led to elevated levels of glucose uptake. These results indicate potential

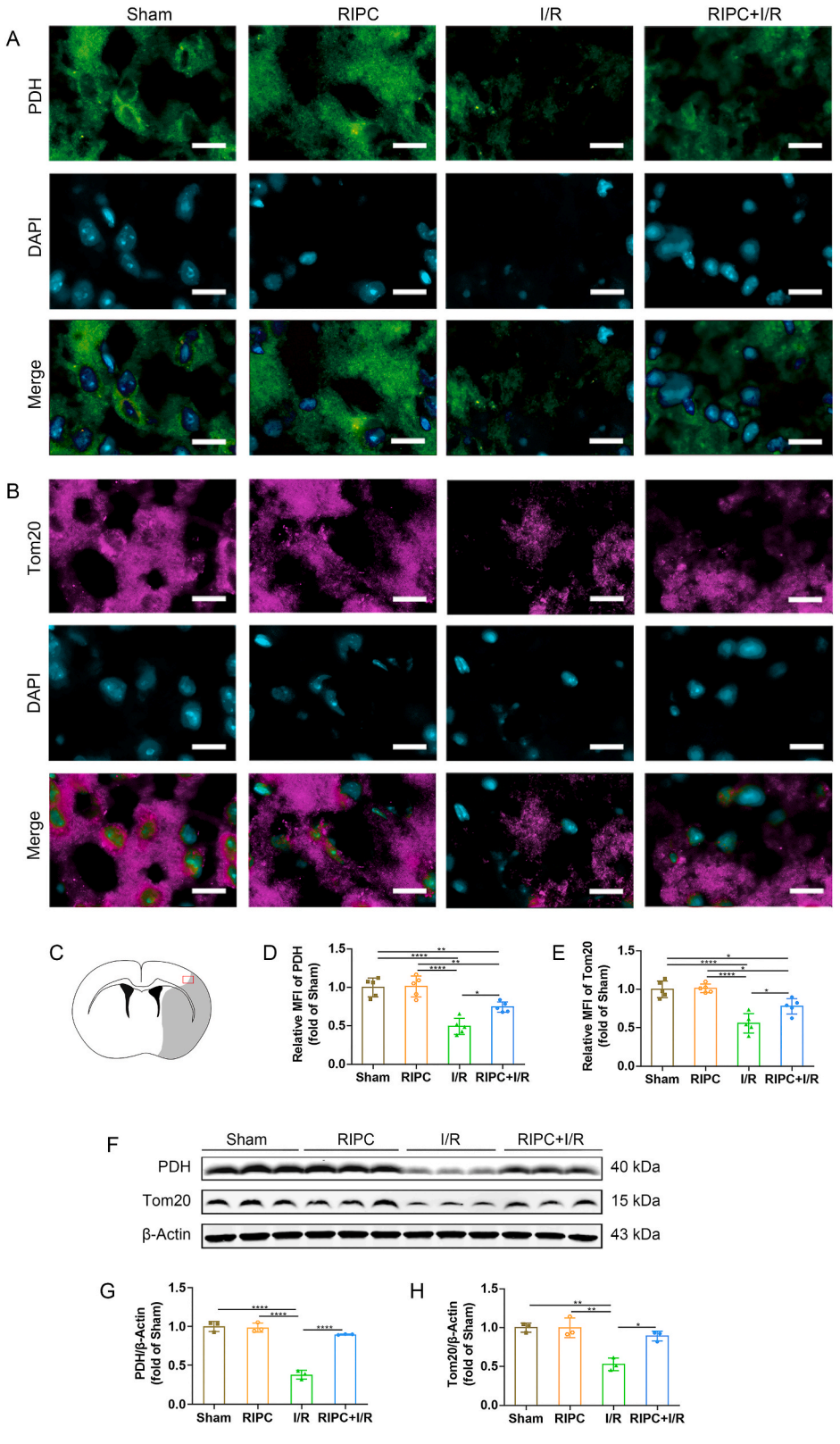

(caption on next page)

Fig. 7. RIPC mitigates mitochondrial damage (A–B) Representative images of PDH and Tom20 immunofluorescence staining for the different groups. (C) The red box in the illustration depicts the ROI in Fig. 7A–B. (D–E) Statistical results of PDH and Tom20 immunofluorescence staining (n = 5 per group). (F) Expressions of PDH and Tom20 proteins detected using Western blot. (G–H) Relative expressions of PDH and Tom20 proteins in the different groups (n = 3 per group). Bar = 25 μm (A, B). Data are presented as mean ± SD (D–E: n = 5; G–H: n = 3). $^{*}P < 0.05$, $^{**}P < 0.01$, $^{***}P < 0.001$, $^{****}P < 0.001$ as determined with ordinary one-way ANOVA (Tukey's multiple comparison test).

enhancement effects on brain function by RIPC treatment. Notably intertwined with energy metabolism processes, glucose uptake relies heavily on mitochondrial activity as a key site for intracellular ATP synthesis [35]. The ADP generated through ATP hydrolysis is subsequently converted into AMP, releasing energy for cellular utilization [36]. Assessing total TAN and the expression levels of Tom20 and PDH offers insights into mitochondrial quality assessment [37–39]. In this experiment, the levels of ATP, ADP, and AMP exhibited a significant decrease in the I/R group, whereas they showed a modest reduction in the RIPC + I/R group. Furthermore, the RIPC + I/R group exhibited elevated levels of the mitochondrial proteins Tom20 and PDH compared to those in the I/R group. It is evident that the function and structure mitochondria of impaired brain tissue in the RIPC + I/R group exhibited significant amelioration, which suggests that RIPC may exert an obvious impact on MQC in I/R mice.

Mitophagy, a selective autophagic process that eliminates damaged mitochondrial, is a crucial mechanism for MQC [23]. Following cerebral I/R, several studies have demonstrated an increase in the ratio of LC3B II/I expression and a decrease in P62 expression [40–42]. However, contrary results have also been reported; specifically, a decrease in the rate of LC3B II/I alongside an increase in P62 expression was observed [43], which may be attributed to variations in the time points studied post-cerebral I/R. In this experiment, we observed a significant down-regulation of P62 protein level and an increased LC3B II/I ratio in the I/R group compared to those in the Sham group. Moreover, there was also a significant decrease in Pink1 and Parkin protein levels, consistent with findings from other researchers [43,44]. These results suggest that a serious degree of mitochondrial autophagy occurs within brain tissue during subacute-stage I/R injury mice, and the PINK1, Parkin, and P62 proteins were excessively degraded. Many neurons exhibit characteristics of autophagy/lysozyme-induced cell death during cerebral ischemic stress [45]. Long-term uncontrolled intense autophagy can lead to cellular apoptosis and death by consuming excessive energy and cellular components [46]. In comparison to the I/R group, both Parkin and P62 protein levels were significantly increased in the RIPC + I/R group, while the LC3B II/I ratio was decreased. Concurrently, co-localization of PDH and LC3B revealed a decreased presence of mitochondrial autophagosomes in the RIPC + I/R group compared to the I/R group.

Our previous experiments have shown that RIPC treatment may exert a neuroprotective role in mice during subacute (2-day) stage following ischemic injury by promoting mitochondria-derived vesicles (MDV) budding events, improving mitochondrial structure, and reducing apoptosis caused by the transfer of AIF and EndoG from mitochondria to nucleus [13]. In this study, it was noted that MDV budding events were rarely observed at the subacute cerebral I/R stage (7-day) after RIPC treatment; however, there was significant improvement in mitochondrial structure and function. This hints that RIPC may employ different mechanisms to regulate MQC during various stages of cerebral I/R. Furthermore, we noted a decrease in mitochondrial autophagosomes and inhibition of autophagy in the RIPC + I/R group compared to the I/R group. Lee et al. reported that certain drugs confer protective effects on ischemia-reperfusion myocardium precisely by reducing mitochondrial division and mitophagy [47]. Although mitophagy is not the primary defense mechanism of MQC system and emerge later, it has been shown to have beneficial effects. Our experiments provide the first evidence that RIPC may play a neuroprotective role by inhibiting excessive mitophagy during subacute cerebral I/R.

There are certain shortcomings in this study. Firstly, it only observed the effects of RIPC on Parkin/PINK1signal, autophagy, mitophagy, mitochondrial structure and function, as well as other brain injury; however, the underlying mechanism requires further elucidation. Secondly, in this experiment, the assessment of mitochondrial structure, function, and mitophagy encompasses all the subtype cells within the detection range of brain, without specifically targeting a particular cell type such as neurons. Additionally, no discernible differences were found between the RIPC group and the Sham group in this study. Therefore, we are unable to explain the changes induced by RIPC produces in normal organisms and its subsequent protective effects during I/R. Future experiments could explore aspects such as proteomics and metabolomics to more comprehensively investigate whether RIPC induces specific "latent" changes that manifest only under stress conditions but remain inconspicuous under normal circumstances.

4. Summary

Despite the limitations of this study, our findings indicate that RIPC may attenuate excessive mitophagy during the subacute (7-day) phase following after ischemic injury. Importantly, our research demonstrates that RIPC treatment enhances mitochondrial structure and function, thereby promoting cell survival while reducing cell and infarct volume. These changes could help to improve brain structure and alleviate symptoms of neurological dysfunction in mice following cerebral I/R (Fig. 9). This study provides important evidence for us to understand why RIPC exerts a protective effect in ischemic events affecting the heart, brain, kidney and other vital organs.

5. Methods

Animals. 93 adult specific pathogen free (SPF) C57BL/6 mice aged 10–12 weeks and weighing 22–25 g were supplied by the Experimental Animal Center at Southwest Medical University. The mice were housed ad libitum in an environment maintained at a temperature of 23 ± 2 °C, indoor relative humidity of 65 ± 5 %, and a 12 h/12 h light/dark cycle. This experiment strictly abided by

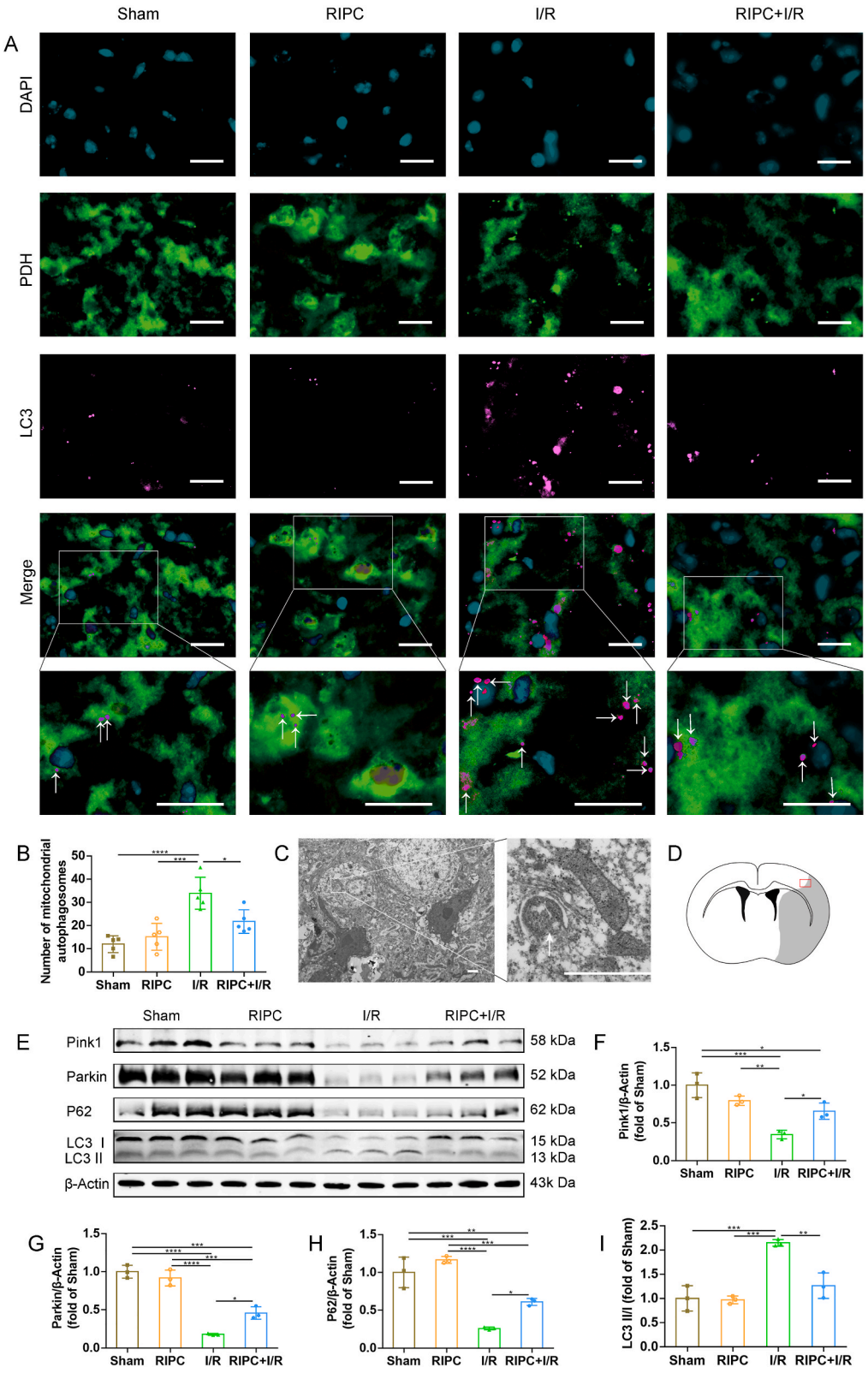

(caption on next page)

Fig. 8. RIPC inhibits mitophagy. (A) Co-localization of PDH and LC3B immunofluorescence staining. The white arrows indicating mitochondrial autophagosomes. (B) Statistical results regarding mitochondrial autophagosomes dual-labeled of PDH and LC3B. (C) Ultrastructure of the mitochondria and mitochondrial autophagosomes in mouse brain following ischemia-reperfusion. The white arrow points to a mitochondrial autophagosome. The red box in the illustration depicts the ROI in Fig. 8A–C. (E) Expression of PINK1, Parkin, P62, and LC3B proteins detected via Western blotting. (F–I) Relative expression levels of PINK1, Parkin, P62 and LC3B proteins in the different groups. Data are presented as mean ± SD (B: n = 5; G–H: n = 3). Bar = 50 μm (A) or 2 μm (C). *$P < 0.05$, ***$P < 0.001$, ****$P < 0.0001$ as determined with ordinary one-way ANOVA (Tukey's multiple comparison test).

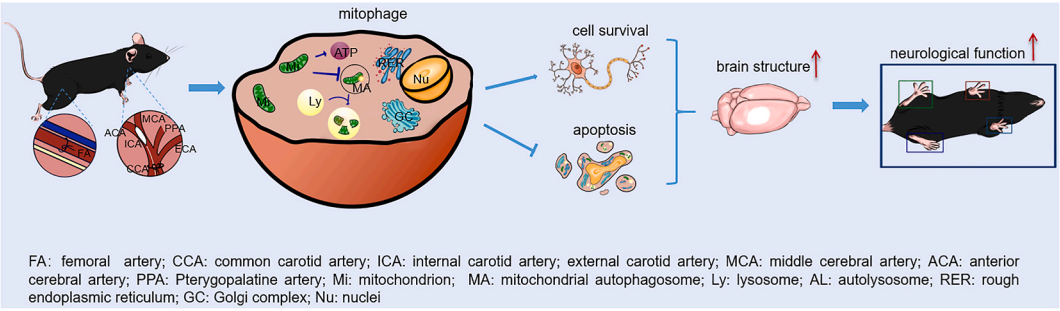

Fig. 9. Graphical summary**.**

the *Regulations on the Management of Experimental Animals* issued by the State Council.

Experimental grouping. The mice were randomly allocated into four groups: the sham operation (Sham) group (n = 23), the cerebral ischemia/reperfusion (I/R) group (n = 23), the RIPC group (n = 23), and the RIPC + I/R group (n = 24). Prior to experimentation, mice were weighed and anesthetized with intraperitoneal injection of 1 % pentobarbital sodium (50 mg/kg). Once anesthetized, they were positioned supine on an operating table. The I/R group underwent middle cerebral artery occlusion (MCAO) for 90 min followed by reperfusion [48]. The Sham group received identical surgical procedure as the I/R mice except without occlusion and reperfusion. In the RIPC group, the mice received ischemic pretreatment as previously reported [13], involving three cycles of bilateral femoral artery occlusion with aneurysm clip for 3 min followed by 5 min of reperfusion. Additionally, the mice did not undergo surgery similar to the sham surgery group. In the RIPC + I/R group, the mice underwent the I/R procedure 48 h after RIPC pretreatment. Following surgery, all mice were placed on a thermostatic mat until they woke up before being returned to their original environment. The animals survived for 9 days after starting the experiment.

Behavioral tests. Mice from each experimental group underwent neurological impairment assessments using the modified Neurological Severity Score (mNSS) test. The test included walking tests, balance beam tests, tail raise tests, and sensory tests, as well as assessment of reflex defects and abnormal movements [49]. A higher total score indicates a more pronounced degree of neurological impairment in the mice.

Gait analysis. On day 9, 8 mice were randomly selected from each group for observation and analysis of their gait using the TreadScan™ gait system (Clever System Inc, USA). The gait parameters assessed in this study included the regularity index of normal step sequence, running speed, print area, stride length, stance and swing time. Mice in the Sham and RIPC groups exhibited consistent running speeds during the training and video recording sessions. In contrast, mice in the I/R group required a longer adaptation period to the track environment during the training and stopped to rest 2–3 times during the 20 s video recording. Mice in the RIPC + I/R group paused for rest 0–3 times.

PET-CT. On day 9, PET/CT imaging was conducted on the brains of mice from four groups using ^{18}F-fluorodeoxyglucose (^{18}F-FDG) positron emission tomography (PET) combined with CT (Siemens, Germany). The procedural specific steps were as follows: (1) Prior to the PET/CT scan, food and water were withheld from the mice for a minimum of 6 h. (2) Following weighing, the mice received peritoneal anesthesia with 1 % pentobarbital sodium. (3) The mice were administered with 50–100 μCi of the ^{18}F-FDG tracer via their tail veins. (4) Forty minutes post-injection, the mice were placed in a prone orientation inside the micro PET/CT instrument with their heads facing the fuselage for whole brain scanning. (5) Analysis and comparison of glucose uptake levels and ischemic focus volumes in each group were performed using ASIPro VM software and PMOD software.

TTC staining. On day 9, 6–7 mice from each experimental group were randomly selected for assessment of tissue ischemia using 1 % 2,3,5-triphenyl tetrazolium chloride (TTC) (Solarbio) at 37 °C. Following staining, the brain sections were fixed with 4 % paraformaldehyde overnight and imaged using a camera. The infarct volume as a percentage of the total volume was analyzed using the ImageJ software.

High-performance liquid chromatography (HPLC). On day 9, adenosine triphosphate (ATP), adenosine diphosphate (ADP), and adenosine monophosphate (AMP) levels in brain tissue were quantified using high-performance liquid chromatography (Shimadzu, Japan). The analysis employed a 250 mm × 4.6 mm * 5 μm chromatographic column (SilGreen ODS AQ) with detection at a wavelength of 260 nm, maintained at a column temperature of 30 °C, and utilizing a sample volume of 10 μL. The gradient elution program and biological sample preparation method adhered to the manufacturer's instructions provided by the kit (Solarbio).

HE staining. On day 9, mice were euthanized after being anesthetized with an overdose of 2 % pentobarbital sodium (100 mg/kg)

and their brain were extracted, fixed with 4 % paraformaldehyde, and then sectioned into 8 μm thick coronal slices following dehydration with a gradient of sucrose solutions. The frozen sections were incubated at 37 °C for 30 min prior to staining with a hematoxylin and eosin solution (Solarbio, G1120) at room temperature.

Nissl staining. The frozen sections were fully immersed in basic dye (Beyotime) at 60°Cfor 30 min in an oven. Subsequently, the excess dye was gradually washed away with running water. The sections underwent dehydration using gradient ethanol solutions, followed by transparency achieved through xylene treatment, and were then observed under a microscope.

TUNEL staining. The sections were incubated with a 20 μg/mL protease K working solution at 37 °C for 15 min, followed by staining using a TdT-mediated dUTP Nick-End Labeling kit (Roche) and DAPI (Solarbio). The staining process was conducted in a light-free environment and sealed with an anti-fluorescence quenching agent.

Immunofluorescence staining. Tissue sections were treated with Triton X-100 and goat serum, followed by overnight incubation at 4 °C with primary antibodies. The antibodies used were anti-pyruvate dehydrogenase (PDH) (1:200, Cell Signal), anti-translocase of the outer membrane 20 (Tom20) (1:200, ThermoFisher), anti-light chain 3B (LC3B) (1:200, Cell Signaling), anti-myelin basic protein (MBP) (1:500, Bioworld), and anti-neuronal nuclei (NeuN) (1:500, ThermoFisher). After washing away excess antibodies with phosphate-buffered solution (PBS), tissue sections were then incubated in a dark environment with goat anti-mouse/rabbit antibody conjugated with a fluorophore (1:1000, Beyotime). Finally, the sections were sealed using an anti-fluorescence quenching agent and imaged using a fluorescence microscope (Olympus, Japan).

Transmission electron microscopy (TEM). On day 9, four mice from each experimental group underwent anesthesia, followed by their brain tissues were quickly removed and stored in 2.5 % glutaraldehyde. Subsequently, the specimens were fixed using 1 % osmium tetroxide, dehydrated through a gradient concentration of acetone, and permeated with a dehydrating agent. The tissue slices were prepared at a thickness of 50 nm and imaged using a JEM-1400 series 120 kV transmission electron microscope (TEM) equipped with an integrated high-sensitivity complementary metal oxide semiconductor (CMOS) camera (JEOL, Japan).

Western Blotting. Three mice from each experimental group were randomly selected for rapid removal of brain tissue, and protein extraction using the RIPA lysate buffer (Solarbio). The brain sample proteins were separated by 10 % SDS–polyacrylamide gel electrophoresis and transferred to PVDF membranes (0.2A, 90min). Subsequently, the membranes were blocked with 3 % skim milk powder, followed by incubated with anti-PDH (1: 1000), anti-Tom20 (1: 1500), anti-PINK1(1: 1000, Abcam), anti-Parkin (1: 1000, Abcam), anti-P62 (1: 1000, Santa Cruz), anti-LC3B (1:1000), and anti-β-Actin (1:10000, Santa Cruz). Then, the membranes were incubated with goat anti-rabbit IgG (1:2000, Beyotime) or anti-mouse IgG (1:2000, Beyotime) second antibody labeled with HRP. Following addition of chemiluminescent liquid to the PVDF membrane, a fluorescence chemiluminescence analyzer was used for exposure and image capture.

6. Statistical analysis

The data were subjected to statistical analysis using GraphPad Prism software, employing one-way ANOVA. The results are presented as the mean ± standard deviation (SD) or triplicates. A significance level of $P < 0.05$ was considered to indicate statistically significant differences between the two groups.

CRediT authorship contribution statement

Jiayi Zhu: Writing – original draft, Software, Methodology, Investigation, Formal analysis, Data curation. **Na Xu:** Writing – original draft, Methodology, Investigation, Data curation. **Heng Lin:** Software, Methodology, Investigation, Data curation. **Li Deng:** Methodology, Formal analysis. **Bingqing Xie:** Writing – original draft, Supervision. **Xiaoqian Jiang:** Methodology, Investigation. **Runde Liao:** Methodology, Investigation. **Chaoxian Yang:** Writing – review & editing, Supervision, Project administration, Funding acquisition, Conceptualization.

Ethics statement

This experimental plan underwent review and approval by Experimental Animal Ethics Committee of Southwest Medical University, which endorsed the procedures for animal care and use (approval number: 20210927-009). The number of the permit issued by the experiment authority is SYXK (Chuan) 2023-0065. The animal experiment was conducted in strict compliance with the guidelines and regulations stipulated by the *State Council's Regulations on the Management of Experimental Animals*.

Data availability statement

Data are available from the corresponding author upon reasonable request.

Funding

This work was supported by the Natural Science Foundation of Sichuan Province (No. 2022NSFSC0718), the Sichuan Science and Technology Program (No. 2022YFS0615), the Application Basic Research Project of Luzhou City of China (2021-JYJ-75) and Applied Basic Project of Southwest Medical University (No. 2021ZKMS011).

Declaration of competing interest

The authors declare no competing interests.

References

[1] S.J. Mendelson, S. Prabhakaran, Diagnosis and management of transient ischemic attack and acute ischemic stroke: a Review, JAMA 325 (11) (2021) 1088–1098.
[2] P. Jolugbo, R.A.S. Ariëns, Thrombus composition and efficacy of thrombolysis and thrombectomy in acute ischemic stroke, Stroke 52 (3) (2021) 1131–1142.
[3] Q. Zhang, P. Deng, S. Chen, H. Xu, Y. Zhang, H. Chen, J. Zhang, H. Sun, Electroacupuncture and human iPSC-derived small extracellular vesicles regulate the gut microbiota in ischemic stroke via the brain-gut axis, Front. Immunol. 14 (2023) 1107559.
[4] J. Liu, Y. Gu, M. Guo, X. Ji, Neuroprotective effects and mechanisms of ischemic/hypoxic preconditioning on neurological diseases, CNS Neurosci. Ther. 27 (8) (2021) 869–882.
[5] M.V. Basalay, S.M. Davidson, A.V. Gourine, D.M. Yellon, Neural mechanisms in remote ischaemic conditioning in the heart and brain: mechanistic and translational aspects, Basic Res. Cardiol. 113 (4) (2018) 25.
[6] D. Sharma, L.N. Maslov, N. Singh, A.S. Jaggi, Remote ischemic preconditioning-induced neuroprotection in cerebral ischemia-reperfusion injury: preclinical evidence and mechanisms, Eur. J. Pharmacol. 883 (2020) 173380.
[7] W. Zhao, S. Li, C. Ren, R. Meng, K. Jin, X. Ji, Remote ischemic conditioning for stroke: clinical data, challenges, and future directions, Ann Clin Transl Neurol 6 (1) (2018) 186–196.
[8] L.F. Saccaro, A. Aimo, M. Emdin, F. Pico, Remote ischemic conditioning in ischemic stroke and myocardial infarction: similarities and differences, Front. Neurol. 12 (2021) 716316.
[9] X. Du, J. Yang, C. Liu, S. Wang, C. Zhang, H. Zhao, H. Du, X. Geng, Hypoxia-inducible factor 1α and 2α have beneficial effects in remote ischemic preconditioning against stroke by modulating inflammatory responses in aged rats, Front. Aging Neurosci. 12 (2020) 54.
[10] J. Mieszkowski, B.E. Stankiewicz, A. Kochanowicz, B. Niespodziński, A.E. Borkowska, K. Sikorska, L. Daniłowicz-Szymanowicz, P. Brzezińska, J. Antosiewicz, Remote ischemic preconditioning reduces marathon-induced oxidative stress and decreases liver and heart injury markers in the serum, Front. Physiol. 12 (2021) 731889.
[11] Z.N. Guo, W.T. Guo, J. Liu, J. Chang, H. Ma, P. Zhang, F.L. Zhang, K. Han, H.H. Hu, H. Jin, X. Sun, D.M. Simpson, Y. Yang, Changes in cerebral autoregulation and blood biomarkers after remote ischemic preconditioning, Neurology 93 (1) (2019) e8–e19.
[12] F. Mayor, A. Bilgin-Freiert, M. Connolly, M. Katsnelson, J.R. Dusick, P. Vespa, S. Koch, N.R. Gonzalez, Effects of remote ischemic preconditioning on the coagulation profile of patients with aneurysmal subarachnoid hemorrhage: a case-control study, Neurosurgery 73 (5) (2013) 808–815. ; discussion 815.
[13] J. Lv, W. Guan, Q. You, L. Deng, Y. Zhu, K. Guo, X. Gao, J. Kong, C. Yang, RIPC provides neuroprotection against ischemic stroke by suppressing apoptosis via the mitochondrial pathway, Sci. Rep. 10 (1) (2020) 5361.
[14] M. Redmann, G.A. Benavides, W.Y. Wani, T.F. Berryhill, X. Ouyang, M.S. Johnson, S. Ravi, K. Mitra, S. Barnes, V.M. Darley-Usmar, J. Zhang, Methods for assessing mitochondrial quality control mechanisms and cellular consequences in cell culture, Redox Biol. 17 (2018) 59–69.
[15] A. Sugiura, G.L. McLelland, E.A. Fon, H.M. McBride, A new pathway for mitochondrial quality control: mitochondrial-derived vesicles, EMBO J. 33 (19) (2014) 2142–2156.
[16] Z. Hu, Y. Yuan, X. Zhang, Y. Lu, N. Dong, X. Jiang, J. Xu, D. Zheng, Human umbilical cord mesenchymal stem cell-derived exosomes attenuate oxygen-glucose deprivation/reperfusion-induced microglial pyroptosis by promoting FOXO3a-dependent mitophagy, Oxid. Med. Cell. Longev. 2021 (2021) 6219715.
[17] Y. Yuan, Y. Zheng, X. Zhang, Y. Chen, X. Wu, J. Wu, Z. Shen, L. Jiang, L. Wang, W. Yang, J. Luo, Z. Qin, W. Hu, Z. Chen, BNIP3L/NIX-mediated mitophagy protects against ischemic brain injury independent of PARK2, Autophagy 13 (10) (2017) 1754–1766.
[18] F. Li, J. Tan, F. Zhou, Z. Hu, B. Yang, Heat shock protein B8 (HSPB8) reduces oxygen-glucose deprivation/reperfusion injury via the induction of mitophagy, Cell. Physiol. Biochem. 48 (4) (2018) 1492–1504.
[19] R. Guan, W. Zou, X. Dai, X. Yu, H. Liu, Q. Chen, W. Teng, Mitophagy, a potential therapeutic target for stroke, J. Biomed. Sci. 25 (1) (2018) 87.
[20] M. Yang, B.S. Linn, Y. Zhang, J. Ren, Mitophagy and mitochondrial integrity in cardiac ischemia-reperfusion injury, Biochim. Biophys. Acta, Mol. Basis Dis. 1865 (9) (2019) 2293–2302.
[21] M. He, T. Zhang, Y. Fan, Y. Ma, J. Zhang, L. Jing, P.A. Li, Deletion of mitochondrial uncoupling protein 2 exacerbates mitophagy and cell apoptosis after cerebral ischemia and reperfusion injury in mice, Int. J. Med. Sci. 17 (17) (2020) 2869–2878.
[22] R. Bolli, The late phase of preconditioning, Circ. Res. 87 (11) (2000) 972–983.
[23] S.P. Loukogeorgakis, A.T. Panagiotidou, M.W. Broadhead, A. Donald, J.E. Deanfield, R.J. MacAllister, Remote ischemic preconditioning provides early and late protection against endothelial ischemia-reperfusion injury in humans: role of the autonomic nervous system, J. Am. Coll. Cardiol. 46 (2005) 450–456.
[24] L. Luo, M. Liu, Y. Fan, J. Zhang, L. Liu, Y. Li, Q. Zhang, H. Xie, C. Jiang, J. Wu, X. Xiao, Y. Wu, Intermittent theta-burst stimulation improves motor function by inhibiting neuronal pyroptosis and regulating microglial polarization via TLR4/NFκB/NLRP3 signaling pathway in cerebral ischemic mice, J. Neuroinflammation 19 (1) (2022) 141.
[25] Y. Zhang, Y. Zhang, X.F. Jin, X.H. Zhou, X.H. Dong, W.T. Yu, W.J. Gao, The role of astragaloside IV against cerebral ischemia/reperfusion injury: suppression of apoptosis via promotion of P62-LC3-autophagy, Molecules 24 (9) (2019) 1838.
[26] P. Zheng, J. Mei, J. Leng, S. Jia, Z. Gu, S. Chen, W. Zhang, A. Cheng, D. Guo, J. Lang, Evaluation of the brain functional activities in rats various location-endometriosis pain model, Ann. Transl. Med. 7 (23) (2019) 767.
[27] J. Zhang, Y. Li, Z. Duan, J. Kang, K. Chen, G. Li, C. Weng, D. Zhang, L. Zhang, J. Wang, B. Li, The effects of the M2a macrophage-induced axonal regeneration of neurons by arginase 1, Biosci. Rep. 40 (2) (2020) BSR20193031.
[28] M. Yuan, Y. Zhang, L. Wang, Y. Hua, Y. Wang, H. Cheng, N. Wang, G. Wang, S. Seto, Study on the mechanism of Tong-Qiao-Huo-Xue decoction regulating apoptosis via ASK1/MKK4/JNK pathway in MCAO/R rats, Phytomedicine 106 (2022) 154437.
[29] S.I. Park, S.K. Park, K.S. Jang, Y.M. Han, C.H. Kim, S.J. Oh, Preischemic neuroprotective effect of minocycline and sodium ozagrel on transient cerebral ischemic rat model, Brain Res. 1599 (2015) 85–92.
[30] W. Wang, T. Wang, W.Y. Feng, Z.Y. Wang, M.S. Cheng, Y.J. Wang, Ecdysterone protects gerbil brain from temporal global cerebral ischemia/reperfusion injury via preventing neuron apoptosis and deactivating astrocytes and microglia cells, Neurosci. Res. 81–82 (2014) 21–29.
[31] M.A.M. Freire, R.R. Lima, L.O. Bittencourt, J.S. Guimaraes, D. Falcao, W. Gomes-Leal, Astrocytosis, inflammation, axonal damage and myelin impairment in the internal capsule following striatal ischemic injury, Cells 12 (3) (2023) 457.
[32] J. Ramos-Cejudo, M. Gutiérrez-Fernández, L. Otero-Ortega, B. Rodríguez-Frutos, B. Fuentes, M.T. Vallejo-Cremades, T.N. Hernanz, S. Cerdán, E. Díez-Tejedor, Brain-derived neurotrophic factor administration mediated oligodendrocyte differentiation and myelin formation in subcortical ischemic stroke, Stroke 46 (1) (2015) 221–228.
[33] A. Bunevicius, H. Yuan, W. Lin, The potential roles of 18F-FDG-PET in management of acute stroke patients, BioMed Res. Int. 2013 (2013) 634598.
[34] X. Jiang, L. Zhou, Z. Sun, B. Xie, H. Lin, X. Gao, L. Deng, C. Yang, MSCs overexpressing GDNF restores brain structure and neurological function in rats with intracerebral hemorrhage, Mol Biomed 4 (1) (2023) 43.
[35] A.J. Roger, S.A. Muñoz-Gómez, R. Kamikawa, The origin and diversification of mitochondria, Curr. Biol. 27 (21) (2017) R1177–R1192.
[36] A. Vergani, S. Tezza, C. Fotino, G. Visner, A. Pileggi, A. Chandraker, P. Fiorina, The purinergic system in allotransplantation, Am. J. Transplant. 14 (3) (2014) 507–514.
[37] J.L. Larson-Casey, C. He, A.B. Carter, Mitochondrial quality control in pulmonary fibrosis, Redox Biol. 33 (2020) 101426.

[38] J. Zhao, D. Qu, Z. Xi, Y. Huan, K. Zhang, C. Yu, D. Yang, J. Kang, W. Lin, S. Wu, Y. Wang, Mitochondria transplantation protects traumatic brain injury via promoting neuronal survival and astrocytic BDNF, Transl. Res. 235 (2021) 102–114.
[39] L. Jia, M. Liao, A. Mou, Q. Zheng, W. Yang, Z. Yu, Y. Cui, X. Xia, Y. Qin, M. Chen, B. Xiao, Rheb-regulated mitochondrial pyruvate metabolism of Schwann cells linked to axon stability, Dev. Cell 56 (21) (2021) 2980–2994.e6.
[40] C. Wang, Z. Ma, Z. Wang, S. Ming, Y. Ding, S. Zhou, H. Qian, Eriodictyol attenuates MCAO-induced brain injury and neurological deficits *via* reversing the autophagy dysfunction, Front. Syst. Neurosci. 15 (2021) 655125.
[41] Q.Y. Zhang, Z.J. Wang, L. Miao, Y. Wang, L.L. Chang, W. Guo, Y.Z. Zhu, Neuroprotective effect of SCM-198 through stabilizing endothelial cell function, Oxid. Med. Cell. Longev. 2019 (2019) 7850154.
[42] E. Sun, J. Zhang, Y. Deng, J. Wang, Q. Wu, W. Chen, X. Ma, S. Chen, X. Xiang, Y. Chen, T. Wu, Y. Yang, B. Chen, Docosahexaenoic acid alleviates brain damage by promoting mitophagy in mice with ischaemic stroke, Oxid. Med. Cell. Longev. 2022 (2022) 3119649.
[43] Y. Jiao, J. Wang, Y. Jia, M. Xue, Remote ischemic preconditioning protects against cerebral ischemia injury in rats by upregulating miR-204-5p and activating the PINK1/Parkin signaling pathway, Metab. Brain Dis. 37 (4) (2022) 945–959.
[44] X. Yu, Y. Luo, L. Yang, P. Chen, X. Duan, P-hydroxybenzyl alcohol ameliorates neuronal cerebral ischemia-reperfusion injury by activating mitochondrial autophagy through SIRT1, Mol. Med. Rep. 27 (3) (2023) 68.
[45] F. Adhami, G. Liao, Y.M. Morozov, A. Schloemer, V.J. Schmithorst, J.N. Lorenz, R.S. Dunn, C.V. Vorhees, M. Wills-Karp, J.L. Degen, R.J. Davis, N. Mizushima, P. Rakic, B.J. Dardzinski, S.K. Holland, F.R. Sharp, C.Y. Kuan, Cerebral ischemia-hypoxia induces intravascular coagulation and autophagy, Am. J. Pathol. 169 (2) (2006) 566–583.
[46] K. Wei, P. Wang, C.Y. Miao, A double-edged sword with therapeutic potential: an updated role of autophagy in ischemic cerebral injury, CNS Neurosci. Ther. 18 (11) (2012) 879–886.
[47] T.L. Lee, M.H. Lee, Y.C. Chen, Y.C. Lee, T.C. Lai, H.Y.H. Lin, L.F. Hsu, H.C. Sung, C.W. Lee, Y.L. Chen, Vitamin D attenuates ischemia/reperfusion-induced cardiac injury by reducing mitochondrial fission and mitophagy, Front. Pharmacol. 11 (2020) 604700.
[48] C. Leithner, M. Füchtemeier, D. Jorks, S. Mueller, U. Dirnagl, G. Royl, Infarct volume prediction by early magnetic resonance imaging in a murine stroke model depends on ischemia duration and time of imaging, Stroke 46 (11) (2015) 3249–3259.
[49] J. Chen, Y. Li, L. Wang, Z. Zhang, D. Lu, M. Lu, M. Chop, Therapeutic benefit of intravenous administration of bone marrow stromal cells after cerebral ischemia in rats, Stroke 32 (4) (2001) 1005–1011.